Efficient 3D inversion of MT data using integral equations method and the receiver footprint approach: application to the large-scale inversion of the EarthScope MT data

Alexander Gribenko, A. Marie Green, Martin Cuma, and Michael S Zhdanov, University of Utah*

SUMMARY

In this paper we present an accurate and efficient method of 3D inversion of MT data. We address two common problems of 3D MT inversion: computational time and memory requirements. The method is based on an IE formulation of the EM forward modeling problem. We apply the quasi-Born approximation to compute the Fréchet derivative. This allows us to use only one rigorous forward modeling per inversion iteration. We have also developed a receiver footprint approach which dramatically reduces the computer memory needed for the Fréchet derivative calculations. We apply our 3D inversion method to the MT data collected in the western United States as a part of the EarthScope project. The inverted electrical conductivity distribution agrees reasonably well with geological features of the region as well as with 3D MT inversion results obtained by other researchers.

INTRODUCTION

During the last decade, a number of 3D magnetotelluric (MT) 3D inversion methods has been developed both for academic and industrial applications (e.g., Sasaki; 2004, Mackie and Watts, 2004). However, many recent magnetotelluric (MT) surveys cover vast regions and contain enormous amounts of data (Green et al., 2008; Patro and Egbert, 2008). Computational time and memory requirements become prohibitive unless one has access to massively parallel electromagnetic (EM) modeling codes and sophisticated cluster hardware. Siripunvaraporn et. al. (2005) and Newman and Alumbaugh (1997) have developed methods of 3D MT inversion for PC clusters. Such computational resources may not be readily available for routine interpretation and research. Maris (2007) developed a method of 3D MT inversion for PCs with multithreaded processors, which provides a faster inverse problem solution, but it still requires a significant amount of memory for storing the sensitivity (Fréchet derivative) matrix.

In this paper we develop an accurate and efficient method of 3D inversion of MT data which addresses two common problems of 3D MT inversion: computational time and memory requirements. Our method is based on an integral equation (IE) formulation of the EM forward modeling problem. We apply the quasi-Born approximation to compute the Fréchet derivative. It is a simplification of the QAVB method described in Gribenko and Zhdanov (2007). We have developed a new receiver footprint approach to reduce the computer memory needed to store the Fréchet derivatives during the inversion process. Our approach is similar to those described in Cox and Zhdanov (2006) for airborne EM data inversion. We tested our method on a simple synthetic model. The test shows that the footprint approach does not practically affect the inversion result. However, the computational cost is reduced dramatically.

The new 3D inversion method is applied to the MT data collected in the framework of the NSF EarthScope project. By the end of 2009 262 MT stations have been collected throughout Oregon, Washington, Idaho, most of Montana and Wyoming as a part of the EarthScope project, 139 of which were used in this analysis. The unique geological structure of Western United States is very important both for the study of its geodynamical history, and for understanding physical processes controlling earthquakes and volcanic eruptions. For such a complex region, definitive structural interpretations based purely on seismological observations may not be sufficient for reliable study of the deep earth interior. Conductivity distribution plays a significant role in determining subsurface tectonic activities because of its sensitivity to temperature, presence of interstitial fluids, melts, volatiles, and bulk composition (Uyeshima et al., 2002). The conductivity features recovered by our inversion can be attributed to regional geological specifications and they show similar conductivity trends compared to other published works.

3D MT INVERSION METHOD

Magnetotelluric inverse problem formulation

We can describe the forward MT problem by an operator equation:

$$\mathbf{d}^{MT} = \mathbf{A}^{MT}(\Delta\sigma), \tag{1}$$

where $\mathbf{d}^{MT}$ stands for a data vector formed by the components of the MT impedance, and $\mathbf{A}^{MT}$ is the nonlinear forward operator symbolizing the governing equations of the MT modeling problem. We use a contraction form of the integral equation method (Hursán and Zhdanov, 2002) for forward modeling of the components of MT impedance. The solution of the problem inverse to (1) can be nonunique and unstable. The conventional way of solving ill-posed inverse problems, according to regularization theory (Tikhonov and Arsenin, 1977, Zhdanov, 2002), is based on minimization of the Tikhonov parametric functional:

$$P^{MT}(\mathbf{m}) = \phi^{MT}(\mathbf{m}) + \alpha S(\mathbf{m}) = min, \tag{2}$$

where $\phi^{MT}(\mathbf{m}) = ||\mathbf{A}^{MT}(\mathbf{m}) - \mathbf{d}^{MT}||_2^2$ is the misfit functional between the predicted data $A^{MT}(\mathbf{m})$ and the observed data $\mathbf{d}^{MT}$, $s(\mathbf{m})$ is a stabilizing functional, and α is a regularization parameter.

We solve this minimization problem using the re-weighted regularized conjugate-gradient (RRCG) method with adaptive regularization parameter selection (Zhdanov, 2002). Our inversion allows different stabilizers, requiring the solution to possess certain properties . The most common choice is the minimum norm (MN) stabilizer, which favors solutions with minimum changes in the produced anomalous conductivity distribution, resulting in a smooth image of the geoelectrical structures. In order to obtain a stable solution with sharp geoelectrical boundaries, we apply focusing stabilizing functionals. Our scheme provides two choices of focusing functionals: minimum-support (MS) (Portniaguine and Zhdanov, 1999) and minimum vertical-support (MVS) stabilizers (Zhdanov et al., 2007).

In order to use the RRCG method for the minimization of the parametric functional (2), it is necessary to calculate the derivative of the data parameters with respect to the model parameters, a Fréchet derivative, sometimes called a Jacobian or sensitivity matrix.

Fréchet derivative calculation

To calculate the derivative of the MT impedances with respect to the anomalous conductivity $\Delta\sigma$, we apply a variational operator to expressions of MT impedance. Resulting partial derivatives of the impedance with respect to the field components are easily obtained by straightforward algebra (Zhdanov, 2009). The Fréchet derivatives of the field components themselves are obtained by so-called quasi-Born (QB) approximation. Gribenko and Zhdanov (2007) described the QAVB method of Fréchet derivative computation. We use a simplified form of QAVB for the case of small conductivity perturbation:

$$\mathbf{F}_{E,H}\left(\mathbf{r}_j \mid \mathbf{r}\right) = \widehat{\mathbf{G}}_{E,H}\left(\mathbf{r}_j \mid \mathbf{r}\right)\mathbf{E}^{(n)}\left(\mathbf{r}\right). \tag{3}$$

For a number of test cases application of QB formula (3) provided comparable accuracy to the QAVB Fréchet derivative. The big advantage of the QB expression is that it results in saving of computational time and, most importantly, in significant computer memory savings. Note that, the electric field $\mathbf{E}^{(n)}$ is computed using the rigorous IE forward modeling method, during the rigorous predicted field computations. Therefore, no extra computation is required to compute the Fréchet derivative.

A footprint approach

To further increase computational speed and reduce computer memory requirements we apply a footprint approach. Cox and Zhdanov (2007) have developed a similar approach for airborne EM data inversion. In the case of conventional inversion, we compute and store full Fréchet derivative matrix, $\mathbf{F}_{i,j}$ with nonzero elements for all MT stations and inversion cells. However, it is obvious that the currents induced in the inversion cells located closer to the station will have a greater effect on the receiver reading than those located further away from the receiver. In fact, at large distances, this input is negligibly small. For this reason, we can compute the Fréchet derivatives for the data observed at a given MT station for the cells located within the station footprint only. Thus, Fréchet derivatives for an MT station can be computed and stored only for regions much smaller than the entire inversion domain, resulting in dramatic reduction of the computer memory requirements.The footprint size is determined based on the skin depth considerations, and depending on the proximity of other MT stations.

We apply the footprint approach for the Fréchet derivative calculation only, and not for the computations of the predicted field. By using all of the cells in the forward modeling computations, we ensure an accurate result for the calculations of both the predicted fields in the receivers and of the electric fields in the domains used in formula (3).

NUMERICAL EXAMPLES

Synthetic model

In the first numerical example we compare the performance of the two inversion methods: a conventional inversion without a footprint and one based on the footprint approach applied to the same synthetic dataset. The model consists of a conductive L-shaped body with a resistivity of 1 Ohm-m located within a resistive homogeneous background with a resistivity of 100 Ohm-m. The synthetic principle MT impedances were computed for 169 MT stations at 16 different frequencies ranging logarithmically between 0.0001 and 10 Hz; for a total number of 5,408 data values. No noise was added to the data in order to see clearly the effects of the footprint. Figure 1 shows a 3D view of the conductive anomaly in the test model for which the synthetic data were computed. We have selected

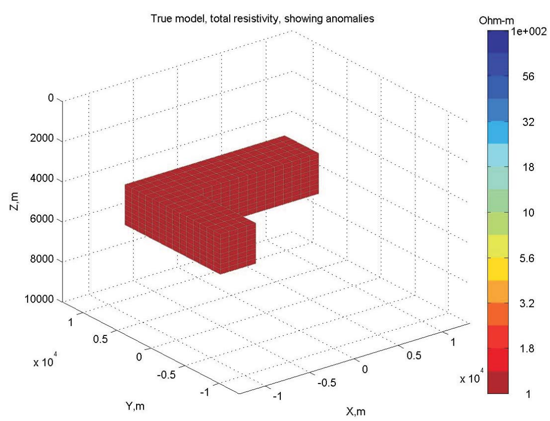

Figure 1: A 3D view of the conductive anomaly in the synthetic model.

an inversion domain with a size of 24 $km \times 24$ $km \times 10$ km in the x, y, and z directions, respectively. The domain was discretized into $23,040$ cells with the size of each cell equal to 1 $km \times 1$ $km \times 0.25$ km. It was impossible to make a finer discretization due to the memory requirements of the nonfootprint inversion. We have applied a conventional inversion algorithm and one based on the footprint approach to the synthetic data computed for this test model. The footprint was defined as a circle with a radius of 10 km. Both conventional and footprint inversions converged to the final 2% relative misfit between the observed and predicted MT impedances after 30 inversion iterations, displaying a very similar convergence character. Figure 2 shows horizontal sections through the models obtained by the inversion. A cross section of the conventional solution is shown side by side with the inverse image obtained using a footprint approach. The results of the two inversions are quite similar, indicating that the footprint approach is valid.

The memory consumption by footprint version of the inversion was reduced by almost 40% compared to the conventional inversion.

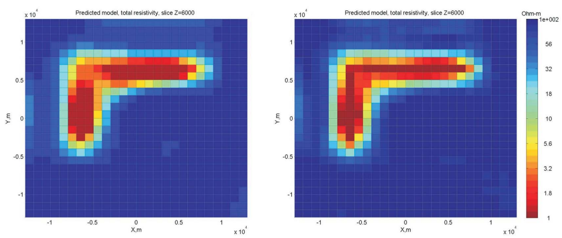

Figure 2: Horizontal sections through the inverse models obtained by a conventional inversion algorithm (left panel) and one based on the footprint approach (right panel).

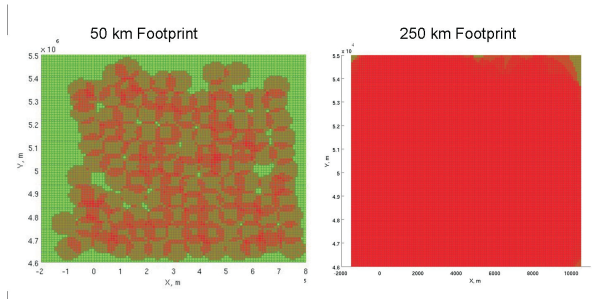

Figure 3: The 50 km receiver footprint on the left is used for preliminary inversion runs and the 250 km receiver footprint on the right is used for final inversion runs. Red regions represent areas with good data coverage and lime green regions show areas with no data coverage.

EarthScope MT data inversion

Figure 2 shows locations of the 232 MT stations partially covering Oregon, Washington, Montana, Idaho, and Wyoming. We inverted principal impedances from 139 stations at 12 frequencies - 0.0002, 0.0004, 0.0007, 0.0012, 0.0019, 0.0029, 0.0046, 0.0076, 0.0117,0.0186, 0.0303, and 0.0508 Hz. The data were selected for inversion based on quality and availability of computational resources. Low frequency MT data can be adversely affected by near-surface conductivity anomalies, which leads to erroneous interpretation (Smith, 1996). Thus as the first step field data were corrected for static shift, using a method described in Green et al., 2008.

For 3D inversion we selected a domain from -150 to 1050 km in the X direction and 4600 to 5500 km in the Y direction. A receiver footprint with radius of 250 km was used to compute and store the Fréchet derivative (Figure 3).

The vertical extent of the inversion domain was down to 700 km, with vertical cell sizes ranging from 0.5 km at the top of the inversion domain to 50 km at the very bottom. The total number of inversion cells was 2,764,800. We extended the inversion domain to a depth greater then the skin depth of the lowest frequency to allow more flexibility and better data fit. The results of inversion below 400 km, however, are considered unreliable. The initial model was selected as a 80 Ohm-m half-space. Inversion was run for 28 smooth iterations and normalized misfit decreased from 27 to 8%. Figure 4 shows an example of the observed and predicted data maps for TM polarization at the frequency of 0.0076 Hz.

North-South and East-West sections through the recovered resistivity distributions are shown in Figures 5 and 6. The main conductive anomaly corresponds well to the location of the Yellowstone plume, recovered from seismic and GPS data (Smith

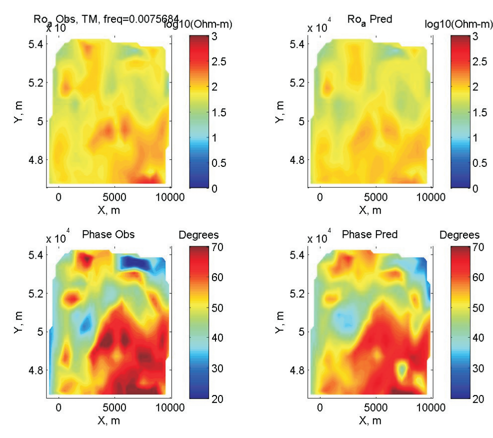

Figure 4: Example of the observed and predicted data maps for TM polarization at the frequency of 0.0076 Hz. Top panels show apparent resistivities, bottom panels show phase. Left panels correspond to the observed data, right panels show predicted data.

et al., 2009). Patro and Egbert, 2008, applied 3D inversion to a subset of the data inverted in this project. Figure 7 shows a comparison of our results with Patro and Egbert's. There is good agreement of shallow conductivity anomalies, which may correspond to the basalts of the Snake river plane.

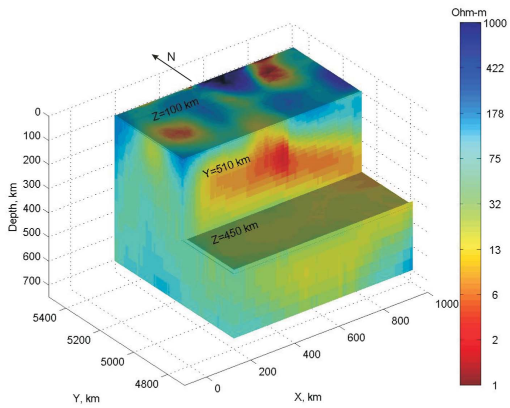

Figure 5: North-South sections through the 3D conductivity distribution recovered by the MT inversion.

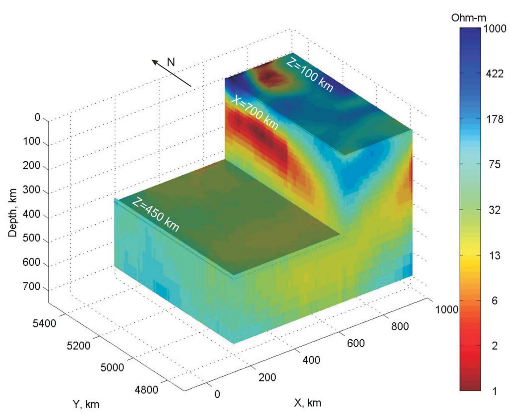

Figure 6: East-West sections through the 3D conductivity distribution recovered by the MT inversion.

CONCLUSIONS

We have developed an accurate and efficient algorithm of 3D inversion of MT data based on the IE method. The quasi-Born approximation, a modification of the QAVB method, speeds up the Fréchet derivative computation significantly, because the domain electric fields computed in the process of rigorous solution of IE equations are re-used to compute the Fréchet derivative. Thus no additional forward modeling is required. The receiver footprint approach has been utilized to dramatically reduce the computer memory needed to store the Fréchet

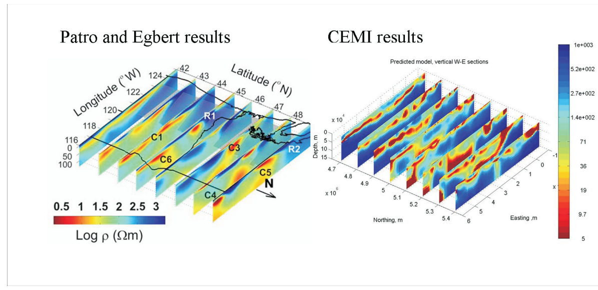

Figure 7: Cross-sectional comparison of Patro and Egbert (2008) results on the left and CEMI results on the right.

derivatives during the inversion process. We have successfully tested our method on a simple synthetic model of a conductive body located within a resistive formation. Synthetic data example shows that the footprint approach produces results very similar to those of the conventional inversion. At the same time, the computational cost is reduced dramatically. An application of the footprint approach allows us to use much finer discretization of the inversion domain in comparison to the conventional 3D MT inversion. We have applied the new method to the regional field MT data, collected as a part of the EarthScope project. Our study demonstrates that the integral equation based inversion method can be successfully applied to real data sets on a regional scale with large data volume. The geoelectrical model obtained as a result of this inversion correlates reasonably well with the available seismic information and published MT inversion results.

ACKNOWLEDGMENTS

The authors acknowledge the support of the University of Utah Consortium for Electromagnetic Modeling and Inversion (CEMI).

Data used in this study were made available through EarthScope (www.earthscope.org; EAR-0323309), supported by the National Science Foundation.

EDITED REFERENCES

Note: This reference list is a copy-edited version of the reference list submitted by the author. Reference lists for the 2010 SEG Technical Program Expanded Abstracts have been copy edited so that references provided with the online metadata for each paper will achieve a high degree of linking to cited sources that appear on the Web.

REFERENCES

Cox, L. H., and M. S. Zhdanov, 2007, Large scale 3D inversion of HEM data using a moving footprint: 77th Annual International Meeting, SEG, Expanded Abstracts, 467-471.

Green, A., A. Gribenko, M. Cuma, and M. S. Zhdanov, 2008, Preliminary results of 3D inversion of the EarthScope Oregon MT data using the integral equation method: Eos, Transactions, American Geophysical Union, **89**, GP51C–08.

Gribenko, A., and M. S. Zhdanov, 2007, Rigorous 3D inversion of marine CSEM data based on the integral equation method: Geophysics, **72**, no. 2, WA73, doi:10.1190/1.2435712.

Hursán, G., and M. S. Zhdanov, 2002, Contraction integral equation method in three-dimensional electromagnetic modeling: Radio Science, **37**, no. 6, 1089-1093, doi:10.1029/2001RS002513.

Mackie, R. L., and M. D. Watts, 2004, The use of 3D magnetotelluric inversion for exploration in complex geologic environments; potential pitfalls and real world examples: Eos, Transactions, American Geophysical Union, **85**, GP14A–01.

Maris, V., 2007, Three-dimensional inversion of magnetotelluric data over the Coso Geothermal Field, using a PC: GRC Transactions, 187-192

Newman, G. A., and D. L. Alumbaugh, 1997, Three-dimensional massively parallel inversion – I. Theory: Geophysical Journal International, **128**, 355–363.

Patro, P. K., and G. D. Egbert, 2008, Regional conductivity structure of Cascadia: Preliminary results from 3D inversion of USArray transportable array magnetotelluric data: Geophysical Research Letters, 35, L20311, doi: 10.1029/ 2008GL035326.

Portniaguine, O. N., and M. S. Zhdanov, 1999, Focusing geophysical inversion images: Geophysics, **64**, 874–887, doi:10.1190/1.1444596.

Sasaki, Y., 2004, Three-dimensional inversion of static-shifted magnetotelluric data: Earth, Planets, and Space, **56**, 239–248.

Siripunvaraporn, W., G. Egbert, Y. Lenbury, and M. Uyeshima, 2005, Three-dimensional magnetotelluric inversion; data-space method: Physics of the Earth and Planetary Interiors, **150**, no. 1-3, 3–14, doi:10.1016/j.pepi.2004.08.023.

Smith, R. B., M. Jordan, B. Steinberger, C. M. Puskas, J. Farrell, G. P. Waite, S. Husen, W. Chang, and R. O'Connell, 2009, Geodynamics of the Yellowstone hotspot and mantle plume: Seismic and GPS imaging, kinematics, and mantle flow: Journal of Volcanology and Geothermal Research, **188**, no. 1-3, 26–56, doi:10.1016/j.jvolgeores.2009.08.020.

Smith, J. T., 1996, Conservative modeling of 3-D electromagnetic fields, Part II: Biconjugate gradient solution and an accelerator: Geophysics, **61**, 1319–1324, doi:10.1190/1.1444055.

Tikhonov, A. N., and V. Y. Arsenin, 1977, Solution of ill-posed problems: V. H. Winston and Sons.

Uyeshima, M., M. Ichiki, I. Fujii, H. Utada, Y. Nishida, H. Satoh, M. Mishina, T. Nishitani, S. Yamaguchi, I. Shiozaki, H. Murakami, and N. Oshiman, 2002, Network-MT Survey in Japan to

Determine Nation-Wide Deep Electrical Conductivity Structure, Seismotectonics in Convergent Plate Boundary, Terra Scientific Publishing Company, 107-121.

Zhdanov, M. S., A. Gribenko, and M. Cuma, 2007, Regularized focusing inversion of marine CSEM data using minimum vertical support stabilizer: Proceedings of the CEMI Annual Meeting, 345-371.

Zhdanov, M. S., 2009, Geophysical electromagnetic theory and methods: Elsevier.

Zhdanov, M. S., 2002, Geophysical inverse theory and regularization problems: Elsevier.